Reverse Time Migration for Reconstructing Extended Obstacles in the Half Space

Zhiming Chen, Guanghui Huang

LSEC, Institute of Computational Mathematics, Academy of Mathematics and Systems Science, Chinese Academy of Sciences, Beijing 100190, China

Abstract. We consider a reverse time migration method for reconstructing extended obstacles in the half space with finite aperture data using acoustic waves at a fixed frequency. We prove the resolution of the reconstruction method in terms of the aperture and the depth of the obstacle embedded in the half space. The resolution analysis implies that the imaginary part of the cross-correlation imaging function always peaks on the illuminated boundary of the obstacle. Numerical experiments are included to illustrate the powerful imaging quality and to confirm our resolution results.

1. Introduction

In this paper we study a reverse time migration (RTM) algorithm to find the support of an unknown obstacle in the half space from the measurement of scattered waves on the boundary of the half space which is far away from the obstacle. The physical properties of the obstacle such as penetrable or non-penetrable, and for non-penetrable obstacles, the type of boundary conditions on the boundary of the obstacle, are not required in the algorithm.

Let the sound soft obstacle occupy a bounded Lipschitz domain $D \subset \mathbb{R}^2_+ = \{(x_1, x_2)^T : x_1 \in \mathbb{R}, x_2 > 0\}$ with ν the unit outer normal to its boundary Γ_D. We assume the incident wave is emitted by a point source located at x_s on the surface $\Gamma_0 = \{(x_1, x_2)^T : x_1 \in \mathbb{R}, x_2 = 0\}$ which is far away from the obstacle. The measured scattering data u is the solution of the following acoustic scattering problem in the half space:

$$\Delta u + k^2 u = -\delta_{x_s}(x) \quad \text{in } \mathbb{R}^2_+ \backslash \bar{D}, \tag{1.1}$$

$$u = 0 \quad \text{on } \Gamma_D, \qquad \frac{\partial u}{\partial x_2} = 0 \quad \text{on } \Gamma_0, \tag{1.2}$$

$$r^{1/2}\left(\frac{\partial u}{\partial r} - \mathbf{i}ku\right) \to 0 \quad \text{as } r = |x| \to \infty, \tag{1.3}$$

where $k > 0$ is the probe wave number, δ_{x_s} is the Dirac source located at x_s. In this paper, by the scattering problem or scattering solution we always mean the solution satisfies the Sommerfeld radiation condition (1.3).

Let $\Phi(x, y) = \frac{\mathbf{i}}{4} H_0^{(1)}(k|x-y|)$ be the fundamental solution of the Helmholtz equation and $N(x, y) = \Phi(x, y) + \Phi(x, y')$ be the Green function of the Helmholtz equation in the half space satisfying the homogeneous Neumann condition on Γ_0, where $y' = (y_1, -y_2)^T$ is the image point of $y = (y_1, y_2)^T \in \mathbb{R}^2_+$. The solution of (1.1)-(1.3) is understood as $u(x, x_s) = N(x, x_s) + u^s(x, x_s)$, where $u^s(x, x_s)$ satisfies Helmholtz equation in $\mathbb{R}^2_+ \backslash \bar{D}$, the radiation condition at infinite, $u^s(x, x_s) = -N(x, x_s)$ on Γ_D, and $\partial u^s(x, x_s)/\partial x_2 = 0$ on Γ_0.

The reverse time migration (RTM) method, which consists of back-propagating the complex conjugated data into the background medium and computing the cross-correlation between the incident wave field and the backpropagated field to output the final imaging profile, is nowadays widely used in exploration geophysics [3, 9, 2]. In [5, 6], the RTM method for reconstructing extended targets using acoustic and electromagnetic waves at a fixed frequency in the free space is proposed and studied. The resolution analysis in [5, 6] is achieved without using the small inclusion or geometrical optics assumption previously made in the literature (e.g. [1, 2]). In [7], a new RTM algorithm is developed for finding extended targets in a planar waveguide which is motivated by the generalized Helmholtz-Kirchhoff identity for scattering problems in waveguides.

In this paper we study a RTM method proposed in [18, 19] for imaging extended obstacles in the half space. This RTM method has the nice feature that it provides true amplitude angle-domain common image gathers. The theoretical study in [19] based

on the geometric optics approximation shows that the imaging functional gives a direct measurement of the angle-dependent reflection coefficient which is rather desirable for geophysical applications [2].

The purpose of this paper is to provide a new mathematical understanding of the RTM method in [18, 19] for extended obstacles without the assumption of geometric optics approximation. We study the resolution of the RTM method for both penetrable and non-penetrable obstacles by extending the analysis in [5, 6] for RTM method in the free space. We introduce the point spread function $J(x, y)$, $x, y \in \mathbb{R}^2_+$, for the half space RTM imaging method and show that this point spread function has the similar features to $J_0(k|x-y|)$, the imaginary part of the fundamental solution of the Helmholtz equation. We also show that the output imaging function is related to the scattering coefficient of the obstacle for incident plane waves.

The rest of this paper is organized as follows. In section 2 we introduce the RTM algorithm. In section 3 we study the point spread function. In section 4 we study the resolution analysis of the RTM method and give the physical interpretation of the imaging function based on the concept of the scattering coefficient. We consider the extension of the resolution results for reconstructing penetrable obstacles or non-penetrable obstacles with impedance boundary conditions in section 5. In section 6 we report extensive numerical experiments to show the competitive performance of the RTM algorithm.

2. Reverse time migration method

In this section we introduce the RTM method for inverse acoustic scattering problems in the half space. Assume that there are N_s sources and N_r receivers uniformly distributed on Γ_0^d, where $\Gamma_0^d = \{(x_1, x_2)^T \in \Gamma_0 : x_1 \in [-d, d]\}$, $d > 0$ is the aperture. We denote by Ω the sampling domain in which the obstacle is sought. Let $h = \text{dist}(\Omega, \Gamma_0)$ be the distance of Ω to Γ_0. We assume the obstacle $D \subset \Omega$ and there exist constants $0 < c_0 < 1, c_1 > 0$ such that

$$|x_1| \leq c_0 d, \quad |x_1 - y_1| \leq c_1 h, \quad \forall x, y \in \Omega. \tag{2.4}$$

The first condition means that the search domain should not be close to the boundary of the aperture. The second condition is rather mild in practical applications as we are interested in finding extended obstacles whose size is comparable or smaller than the probe wavelength and h, the distance of the obstacle to Γ_0, is large compared with the probe wavelength, i.e., $kh \gg 1$. In the following we also assume $d \geq h$.

Our RTM algorithm consists of two steps [18, 19]. The first step is the back-propagation in which we back-propagate the complex conjugated data $\overline{u^s(x_r, x_s)}$ as the Dirichlet boundary condition into the domain. The second step is the cross-correlation in which we compute the imaginary part of the cross-correlation of the back-propagated field and the incoming wave which uses the source as the boundary condition on Γ_0.

Algorithm 2.1 (Reverse time migration)
Given the data $u^s(x_r, x_s)$ which is the measurement of the scattered field at $x_r = (x_1(x_r), x_2(x_r))^T$ when the source is emitted at $x_s = (x_1(x_s), x_2(x_s))^T$, $s = 1, \ldots, N_s$, $r = 1, \ldots, N_r$.
1° *Back-propagation: For $s = 1, \ldots, N_s$, compute the back-propagation field*

$$v_b(z, x_s) = \frac{|\Gamma_0^d|}{N_r} \sum_{r=1}^{N_r} \frac{\partial \Phi(x_r, z)}{\partial x_2(x_r)} \overline{u^s(x_r, x_s)}, \qquad \forall\ z \in \Omega. \tag{2.5}$$

2° *Cross-correlation: For $z \in \Omega$, compute*

$$I_d(z) = \mathrm{Im} \left\{ \frac{|\Gamma_0^d|}{N_s} \sum_{s=1}^{N_s} \frac{\partial \Phi(x_s, z)}{\partial x_2(x_s)} v_b(z, x_s) \right\}. \tag{2.6}$$

It is easy to see that

$$I_d(z) = \mathrm{Im} \left\{ \frac{|\Gamma_0^d||\Gamma_0^d|}{N_s N_r} \sum_{s=1}^{N_s} \sum_{r=1}^{N_r} \frac{\partial \Phi(x_s, z)}{\partial x_2(x_s)} \frac{\partial \Phi(x_r, z)}{\partial x_2(x_r)} \overline{u^s(x_r, x_s)} \right\}, \qquad \forall\ z \in \Omega. \tag{2.7}$$

This formula is used in all our numerical experiments in section 6. By letting $N_s, N_r \to \infty$, we know that (2.7) can be viewed as an approximation of the following continuous integral:

$$\hat{I}_d(z) = \mathrm{Im} \int_{\Gamma_0^d} \int_{\Gamma_0^d} \frac{\partial \Phi(x_s, z)}{\partial x_2(x_s)} \frac{\partial \Phi(x_r, z)}{\partial x_2(x_r)} \overline{u^s(x_r, x_s)} ds(x_r) ds(x_s), \qquad \forall\ z \in \Omega. \tag{2.8}$$

For $x, y \in \mathbb{R}^2_+$, let $G(x, y) = \Phi(x, y) - \Phi(x, y')$ be the Green function of the Helmholtz equation in the half space satisfying the homogeneous Dirichlet condition on Γ_0, where $y' = (y_1, -y_2)^T$ is the image point of y. Since $\frac{\partial G(x_s, z)}{\partial x_2(x_s)} = 2\frac{\partial \Phi(x_s, z)}{\partial x_2(x_s)}$ and $\frac{\partial G(x_r, z)}{\partial x_2(x_r)} = 2\frac{\partial \Phi(x_r, z)}{\partial x_2(x_r)}$ for $x_s, x_r \in \Gamma_0$. The imaging function proposed in [18, 19] is exactly the limit of $\hat{I}_d(z)$ as $d \to \infty$. We will study the resolution of the function $\hat{I}_d(z)$ in the section 4. To this end we will first consider the resolution of the finite aperture point source function in the next section.

3. The point spread function

We start by introducing some notation. For any bounded domain $U \subset \mathbb{R}^2$ with Lipschitz boundary Γ, we will use the weighted $H^1(U)$ norm $\|u\|_{H^1(U)} = (\|\nabla \phi\|^2_{L^2(U)} + d_U^{-2}\|\phi\|^2_{L^2(U)})^{1/2}$ and the weighted $H^{1/2}(\Gamma)$ norm $\|v\|_{H^{1/2}(\Gamma)} = (d_U^{-1}\|v\|^2_{L^2(\Gamma)} + |v|^2_{\frac{1}{2},\Gamma})^{1/2}$, where d_U is the diameter of U and

$$|v|_{\frac{1}{2},\Gamma} = \left(\int_\Gamma \int_\Gamma \frac{|v(x) - v(y)|^2}{|x - y|^2} ds(x) ds(y) \right)^{1/2}.$$

By the scaling argument and the trace theorem we know that there exist constants $C_1, C_2 > 0$ independent of d_U such that for any $v \in H^{1/2}(\Gamma)$,

$$C_1 \frac{|U|^{\frac{1}{2}}}{|\Gamma|} \|v\|_{H^{1/2}(\Gamma)} \le \inf_{\phi|_\Gamma = v,\, \phi \in H^1(U)} \|\phi\|_{H^1(U)} \le C_2 \frac{|U|^{\frac{1}{2}}}{d_U} \|v\|_{H^{1/2}(\Gamma)}. \tag{3.9}$$

The point spread function measures the resolution for finding a point source [1]. We introduce the following point spread function for half space inverse scattering problems:

$$J(z,y)=\int_{\Gamma_0}\frac{\partial G(x,z)}{\partial x_2}\overline{N(x,y)}ds(x),\quad \forall z,y\in\mathbb{R}^2_+. \tag{3.10}$$

This point spread function states that for finding the point source $y\in\mathbb{R}^2_+$, the received data $\overline{N(x,y)}$, $x\in\Gamma_0$, is back-propagated to the domain $\mathbb{R}^2_+$ as the Dirichlet boundary condition. Since $\frac{\partial G(x,z)}{\partial x_2}=2\frac{\partial \Phi(x,z)}{\partial x_2}$ and $N(x,y)=2\Phi(x,y)$ for $x\in\Gamma_0$, we have

$$J(z,y)=4\int_{\Gamma_0}\frac{\partial \Phi(x,z)}{\partial x_2}\overline{\Phi(x,y)}ds(x),\quad \forall z,y\in\mathbb{R}^2_+. \tag{3.11}$$

Lemma 3.1 *For any $z,y\in\mathbb{R}^2_+$, $J(z,y)=F(z,y)+R(z,y)$, where*

$$F(z,y)=-\frac{\mathbf{i}}{2\pi}\int_0^{\pi}e^{\mathbf{i}k(z_1-y_1)\cos\theta+\mathbf{i}k(z_2-y_2)\sin\theta}d\theta, \tag{3.12}$$

$$R(z,y)=\frac{1}{\pi}\int_k^{+\infty}\frac{1}{\sqrt{\xi_1^2-k^2}}e^{-\sqrt{\xi_1^2-k^2}(z_2+y_2)}\cos(\xi_1(z_1-y_1))d\xi_1. \tag{3.13}$$

Moreover, $|R(z,y)|+k^{-1}|\nabla_y R(z,y)|\le\frac{1}{\pi k(z_2+y_2)}$ uniformly for $z,y\in\mathbb{R}^2_+$.

Proof. By the limiting absorption principle $\Phi(x,y)$ is the limit of the fundamental solution $\Phi_\varepsilon(x,y)$ of the Helmholtz equation with the complex wave number $k+\mathbf{i}\varepsilon$ as $\varepsilon\to 0$. It is easy to see that [8, P. 59]

$$\Phi_\varepsilon(x,y)=\frac{1}{2\pi}\int_{-\infty}^{+\infty}\frac{\mathbf{i}}{2\mu_\varepsilon}e^{\mathbf{i}\mu_\varepsilon|x_2-y_2|+\mathbf{i}\xi_1(x_1-y_1)}d\xi_1,$$

where $\mu_\varepsilon=((k+\mathbf{i}\varepsilon)^2-\xi_1^2)^{1/2}$. Here we take the branch cut of the complex plane such that $\mathrm{Re}\,(z^{1/2})\ge 0$ for any $z\in\mathbb{C}\backslash\{0\}$.

Applying the Fourier transformation to the first horizontal variable of $\Phi_\varepsilon(x,y)$, we have

$$\mathcal{F}[\Phi_\varepsilon](\xi_1,x_2;y_1,y_2)=\frac{\mathbf{i}}{2\mu_\varepsilon}e^{\mathbf{i}\mu_\varepsilon|x_2-y_2|}e^{-\mathbf{i}\xi_1 y_1},$$

$$\mathcal{F}\left[\frac{\partial\Phi_\varepsilon}{\partial x_2}\right](\xi_1,x_2;z_1,z_2)=\frac{1}{2}\mathrm{sgn}(z_2-x_2)e^{\mathbf{i}\mu_\varepsilon|x_2-z_2|}e^{-\mathbf{i}\xi_1 z_1}.$$

Using Parseval identity combined with the above two equations, we know that

$$\begin{aligned}J_\varepsilon(z,y):&=4\int_{-\infty}^{\infty}\left[\frac{\partial\Phi_\varepsilon(x,z)}{\partial x_2}\overline{\Phi_\varepsilon(x,y)}\right]_{x_2=0}dx_1\\&=\frac{2}{\pi}\left\langle\mathcal{F}\left[\frac{\partial\Phi_\varepsilon}{\partial x_2}\right](\cdot,0;z_1,z_2),\mathcal{F}[\Phi_\varepsilon](\cdot,0;y_1,y_2)\right\rangle\\&=-\frac{\mathbf{i}}{2\pi}\int_{-\infty}^{\infty}\frac{1}{\bar\mu_\varepsilon}e^{\mathbf{i}\mu_\varepsilon z_2-\mathbf{i}\bar\mu_\varepsilon y_2+\mathbf{i}\xi_1(y_1-z_1)}d\xi_1.\end{aligned}$$

This implies by letting $\varepsilon\to 0$ and using (3.11) that

$$J(z,y)=-\frac{\mathbf{i}}{2\pi}\int_{-k}^{k}\frac{1}{\mu}e^{\mathbf{i}\mu(z_2-y_2)-\mathbf{i}\xi_1(z_1-y_1)}d\xi_1+R(z,y),$$

where $\mu = (k^2 - \xi_1^2)^{1/2}$. Finally, it is easy to check that

$$|R(z,y)| \le \frac{1}{\pi k(z_2+y_2)}, \quad \left|\frac{\partial R(z,y)}{\partial y_j}\right| \le \frac{1}{\pi(z_2+y_2)}, \quad j=1,2,$$

for any $z, y \in \mathbb{R}^2_+$. This completes the proof. □

Figure 1 shows the surface plot of the point spread function $J(z,y)$. Lemma 3.1 indicates that for z, y far away from Γ_0, the main contribution to the point spread function is from $F(z,y)$. Our next goal is to show that $F(z,y)$ has the similar decay behavior to the Bessel function $J_0(k|z-y|)$ as $|z-y| \to \infty$. We need the following slight generalization of Van der Corput lemma for the oscillatory integral [12, P.152].

Lemma 3.2 *Let $-\infty < a < b < \infty$, $\lambda > 0$, and u is a C^2 function in $]a,b[$.*
1° If $|u''(t)| \ge 1$ for $t \in]a,b[$, then there exists a constant C independent of λ, a, b, u such that $|\int_a^b e^{\mathbf{i}\lambda u(t)} dt| \le C\lambda^{-1/2}$.
2° If $|u'(t)| \ge 1$ for $t \in]a,b[$ and u' is monotone in $]a,b[$, then $|\int_a^b e^{\mathbf{i}\lambda u(t)} dt| \le 3\lambda^{-1}$.

Proof. The assertion 1° is in [12, Exercise 2.6.1] which can be proved by extending the argument for the case $u''(t) \ge 1$ of the Van der Corput lemma. The assertion 2° can be proved by extending the argument for the case $u'(t) \ge 1$ of the Van der Corput lemma. Here we omit the details. □

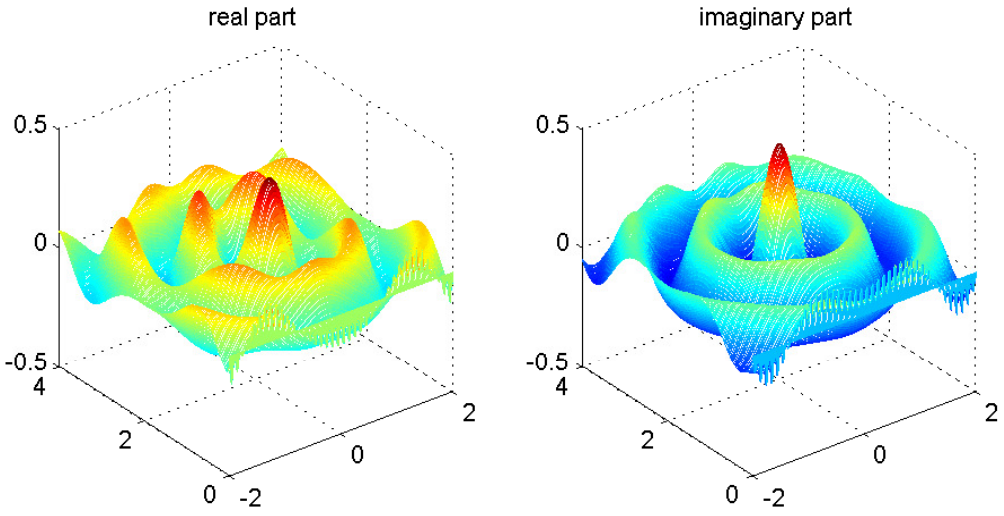

Figure 1. The surface plot of the point spread imaging function $J(z,y)$ ($z \in [-2,2] \times [0,4], y = (0,2)^T$) for $k = 2\pi$: real part (left) and imaginary part (right).

Lemma 3.3 *For any $z, y \in \mathbb{R}^2_+$, $F(z,y) = -\mathbf{i}/2$ when $z = y$ and for $z \ne y$,*

$$|F(z,y)| \le C\left[(k|z-y|)^{-1/2} + (k|z-y|)^{-1}\right].$$

where the constant C is independent of $k, |z-y|$.

Proof. It is obvious that $F(z,y) = -\mathbf{i}/2$ when $z = y$. For $z \neq y$, we denote $y - z = |y - z|(\cos\phi, \sin\phi)^T$ for some $0 \leq \phi < 2\pi$. Then it is easy to see that

$$F(z,y) = -\frac{\mathbf{i}}{2\pi}\int_0^\pi e^{\mathbf{i}k|z-y|\cos(\theta-\phi)}d\theta.$$

The phase function $f(\theta) = \cos(\theta-\phi)$ satisfies $f'(\theta) = -\sin(\theta-\phi)$, $f''(\theta) = -\cos(\theta-\phi)$. For any given $0 \leq \phi < 2\pi$, we can decompose $]0,\pi[$ into several intervals such that in each interval either $|f''(\theta)| \geq 1/2$ or $|f'(\theta)| \geq 1/2$ and $f'(\theta)$ is monotone. The estimate for $F(z,y)$ follows by using Lemma 3.2. □

The following consequence of Lemma 3.1 and Lemma 3.3 will be used in the next section.

Corollary 3.1 *There exists a constant C independent of k,h such that*

$$\|F(z,\cdot)\|_{H^{1/2}(\Gamma_D)} + \|\partial F(z,\cdot)/\partial\nu\|_{H^{-1/2}(\Gamma_D)} \leq C(1+kd_D),$$
$$\|R(z,\cdot)\|_{H^{1/2}(\Gamma_D)} + \|\partial R(z,\cdot)/\partial\nu\|_{H^{-1/2}(\Gamma_D)} \leq C(1+kd_D)(kh)^{-1},$$

uniformly for $z \in \Omega$, where d_D is the diameter of the obstacle D.

Proof. We first observe that for any function $\phi \in H^1(D)$, by (3.9),

$$\|\phi\|_{H^{1/2}(\Gamma_D)} \leq C(d_D^{-1}\|\phi\|_{L^2(D)} + \|\nabla\phi\|_{L^2(D)}) \leq C\max_{x\in D}(|\phi(x)| + d_D|\nabla\phi(x)|). \tag{3.14}$$

Next by the definition of the $H^{-1/2}(\Gamma_D)$ norm we have

$$\|\partial\phi/\partial\nu\|_{H^{-1/2}(\Gamma_D)} \leq Cd_D^{1/2}\|\partial\phi/\partial\nu\|_{L^2(\Gamma_D)} \leq Cd_D\max_{x\in D}|\nabla\phi(x)|. \tag{3.15}$$

Now the estimate for $F(z,\cdot)$ follows from the fact that $|F(z,y)| \leq 1/2, |\nabla_y F(z,y)| \leq k/2$ for any $z, y \in \Omega$. The estimate for $R(z,\cdot)$ follows from Lemma 3.1. □

Now we consider the finite aperture point spread function $J_d(z,y)$:

$$J_d(z,y) = \int_{-d}^{d}\left[\frac{\partial G(x,z)}{\partial x_2}\overline{N(x,y)}\right]_{x_2=0} dx_1. \tag{3.16}$$

Our aim is to estimate the difference $J(z,y) - J_d(z,y)$. We first recall the following estimate for the first kind Hankel function [4, (1.22)-(1.23)].

Lemma 3.4 *For any $t > 0$, we have*

$$|H_0^{(1)}(t)| \leq \left(\frac{2}{\pi t}\right)^{1/2}, |H_1^{(1)}(t)| \leq \left(\frac{2}{\pi t}\right)^{1/2} + \frac{2}{\pi t}.$$

Theorem 3.1 *Assume $d \geq h$, for any $z, y \in \Omega$, we have*

$$|J(z,y) - J_d(z,y)| + k^{-1}|\nabla_y(J(z,y) - J_d(z,y))| \leq C\Big(\frac{h}{d}\Big),$$

where the constant C is independent of k, h, d.

Proof. By definition we have

$$J(z,y) - J_d(z,y) = 4 \int_{(-\infty,-d)\cup(d,+\infty)} \left[\frac{\partial \Phi(x,z)}{\partial x_2} \overline{\Phi(x,y)} \right]_{x_2=0} dx_1. \tag{3.17}$$

Notice that for any $z \in \mathbb{R}^2_+$, $x \in \Gamma_0$,

$$\frac{\partial \Phi(x,z)}{\partial x_2} = \frac{\mathbf{i}}{4} H_1^{(1)}(k|x-z|) \frac{kz_2}{|x-z|}. \tag{3.18}$$

By Lemma 3.4, we have

$$\begin{aligned} &\left| \int_d^{+\infty} \left[\frac{\partial \Phi(x,z)}{\partial x_2} \overline{\Phi(x,y)} \right]_{x_2=0} dx_1 \right| \\ &\leq \int_d^{+\infty} \left[\frac{kz_2}{16|x-z|} \left(\left(\frac{2}{k\pi|x-z|} \right)^{1/2} + \frac{2}{k\pi|x-z|} \right) \left(\frac{2}{k\pi|x-y|} \right)^{1/2} \right]_{x_2=0} dx_1 \\ &\leq C \left(\frac{h}{d} \right). \end{aligned}$$

Here we have used the first inequality in (2.4). Similarly, we can prove that the estimate for the integral in $]-\infty, d[$ in (3.17). This shows the estimate for $J(z,y) - J_d(z,y)$. The estimate for $\nabla_y (J(z,y) - J_d(z,y))$ can be proved similarly. □

By (3.14)-(3.15) we obtain the following corollary.

Corollary 3.2 *There exists a constant C independent of k,h such that*

$$\|J(z,\cdot) - J_d(z,\cdot)\|_{H^{1/2}(\Gamma_D)} + \|\partial (J(z,\cdot) - J_d(z,\cdot))/\partial \nu\|_{H^{-1/2}(\Gamma_D)} \leq C(1+kd_D) \left(\frac{h}{d} \right).$$

uniformly for $z \in \Omega$, where d_D is the diameter of the obstacle D.

4. The resolution analysis

In this section we study the imaging resolution of the RTM Algorithm 2.1 for the sound soft obstacle in the half space. We first introduce the following stability estimate of the forward acoustic scattering problem in the half space which can be proved by the limiting absorption principle by extending the classical argument in [14, 7].

Lemma 4.1 *Let $g \in H^{1/2}(\Gamma_D)$, then the scattering problem of Helmholtz equation in the half space*

$$\Delta u + k^2 u = 0 \ \text{ in } \mathbb{R}^2_+ \backslash \bar{D}, \qquad u = g \ \text{ on } \Gamma_D, \qquad \frac{\partial u}{\partial x_2} = 0 \ \text{ on } \Gamma_0, \tag{4.19}$$

has a unique solution $u \in H^1_{\text{loc}}(\mathbb{R}^2_+ \backslash \bar{D})$. Moreover, there exists a constant $C > 0$ such that $\|\partial u/\partial \nu\|_{H^{-1/2}(\Gamma_D)} \leq C \|g\|_{H^{1/2}(\Gamma_D)}$.

The following theorem shows that the difference between the half space scattering solution and the full space scattering solution is small if the scatterer is far away from the boundary Γ_0. The theorem will be proved in the appendix of this paper.

Theorem 4.1 *Let $g \in H^{1/2}(\Gamma_D)$ and u_1, u_2 be the scattering solutions of following problems:*

$$\Delta u_1 + k^2 u_1 = 0 \ \text{ in } \mathbb{R}^2_+\backslash\bar{D}, \quad u_1 = g \ \text{ on } \Gamma_D, \quad \frac{\partial u_1}{\partial \nu} = 0 \ \text{ on } \Gamma_0, \tag{4.20}$$

$$\Delta u_2 + k^2 u_2 = 0 \ \text{ in } \mathbb{R}^2\backslash\bar{D}, \quad u_2 = g \ \text{ on } \Gamma_D. \tag{4.21}$$

Then there exists a constant C such that $\|\partial(u_1 - u_2)/\partial\nu\|_{H^{-1/2}(\Gamma_D)} \le C(1 + kd_D)^2(kh)^{-1/2}\|g\|_{H^{1/2}(\Gamma_D)}$.

The following theorem is the main result of this section.

Theorem 4.2 *For any $z \in \Omega$, let $\psi(y, z)$ be the scattering solution to the following problem:*

$$\Delta_y \psi(y,z) + k^2\psi(y,z) = 0 \quad \text{in } \mathbb{R}^2\backslash\bar{D}, \qquad \psi(y,z) = -\overline{F(z,y)} \ \text{ on } \Gamma_D. \tag{4.22}$$

Then, we have

$$\hat{I}_d(z) = \frac{1}{4}\,\mathrm{Im}\Big\{\int_{\Gamma_D} \frac{\partial(F(z,y) + \psi(y,z))}{\partial\nu(y)}\overline{F(z,y)}ds(y)\Big\} + W_{\hat{I}}(z), \tag{4.23}$$

where $|W_{\hat{I}}(z)| \le C(1 + kd_D)^4((kh)^{-1/2} + h/d)$ uniformly for z in Ω.

Proof. By the integral representation, we have,

$$u^s(x_r, x_s) = \int_{\Gamma_D}\left(u^s(y,x_s)\frac{\partial N(x_r,y)}{\partial\nu(y)} - \frac{\partial u^s(y,x_s)}{\partial\nu(y)}N(x_r,y)\right)ds(y).$$

From (3.16) we get for any $z \in \Omega$,

$$\begin{aligned}&\int_{\Gamma_0^d}\frac{\partial\Phi(x_r,z)}{\partial x_2(x_r)}\overline{u^s(x_r,x_s)}ds(x_r)\\ &= \frac{1}{2}\int_{\Gamma_D}\Big[\overline{u^s(y,x_s)}\frac{\partial J_d(z,y)}{\partial\nu(y)} - \frac{\partial\overline{u^s(y,x_s)}}{\partial\nu(y)}J_d(z,y)\Big]ds(y).\end{aligned}$$

By the definition of the imaging function $\hat{I}_d(z)$, we have then

$$\hat{I}_d(z) = \frac{1}{4}\,\mathrm{Im}\int_{\Gamma_D}\Big[v_s(y,z)\frac{\partial J_d(z,y)}{\partial\nu(y)} - \frac{\partial v_s(y,z)}{\partial\nu(y)}J_d(z,y)\Big]ds(y), \tag{4.24}$$

where $v_s(y,z) = 2\int_{\Gamma_0^d}\frac{\partial\Phi(x_s,z)}{\partial x_2(x_s)}\overline{u^s(y,x_s)}ds(x_s)$. Taking the complex conjugate we get

$$\overline{v_s(y,z)} = 2\int_{\Gamma_0^d}\frac{\partial\overline{\Phi(x_s,z)}}{\partial x_2(x_s)}u^s(y,x_s)ds(x_s).$$

Therefore, $\overline{v_s(y,z)}$ can be viewed as the weighted superposition of $u^s(y,x_s)$. Then $\overline{v_s(y,z)}$ satisfies the Helmholtz equation

$$\Delta_y\overline{v_s(y,z)} + k^2\overline{v_s(y,z)} = 0 \quad \text{in } \mathbb{R}^2_+\backslash\bar{D}.$$

On the boundary of the obstacle Γ_D, we have

$$\begin{aligned}\overline{v_s(y,z)} &= 2\int_{\Gamma_0^d} \frac{\partial\overline{\Phi(x_s,z)}}{\partial x_2(x_s)} u^s(y,x_s)ds(x_s)\\ &= -2\int_{\Gamma_0^d} \frac{\partial\overline{\Phi(x_s,z)}}{\partial x_2(x_s)} N(y,x_s)ds(x_s)\\ &= -\overline{J_d(z,y)}, \quad \forall y\in\Gamma_D.\end{aligned}$$

Moreover, $\partial\overline{v_s(y,z)}/\partial y_2 = 0$ on Γ_0 since $\partial u^s(y,x_s)/\partial y_2 = 0$ on Γ_0. Let $w_d(y,z)$ be the scattering solution of the problem:

$$\begin{aligned}&\Delta_y w_d(y,z) + k^2 w_d(y,z) = 0 \ \text{ in } \mathbb{R}^2_+\backslash\bar{D},\\ &w_d(y,z) = \overline{F(z,y)} - \overline{J_d(z,y)} \ \text{ on } \Gamma_D, \quad \frac{\partial w_d(y,z)}{\partial y_2} = 0 \ \text{ on } \Gamma_0.\end{aligned}$$

By Lemma 4.1 and Corollaries 3.1-3.2 we have

$$\begin{aligned}\|\partial w_d(\cdot,z)/\partial\nu\|_{H^{-1/2}(\Gamma_D)} &\le C\|F(z,\cdot) - J_d(z,\cdot)\|_{H^{1/2}(\Gamma_D)}\\ &\le C(1+kd_D)((kh)^{-1} + h/d).\end{aligned} \tag{4.25}$$

Let $w(y,z) := \overline{v_s(y,z)} - w_d(y,z) - \psi(y,z)$. Since $\overline{v_s(y,z)} - w_d(y,z)$ satisfies the half-space scattering problem (4.20) with $g(y) = -\overline{F(z,y)}$, by using Theorem 4.1 and Corollary 3.1,

$$\begin{aligned}\|\partial w(\cdot,z)/\partial\nu\|_{H^{-1/2}(\Gamma_D)} &\le C(1+kd_D)^2(kh)^{-1/2}\|F(z,\cdot)\|_{H^{1/2}(\Gamma_D)}\\ &\le C(1+kd_D)^3(kh)^{-1/2}.\end{aligned} \tag{4.26}$$

Now we substitute $\overline{v_s(y,z)} = \psi(y,z) + w(y,z) + w_d(y,z)$ into (4.24) to obtain,

$$\hat{I}_d(z) = \frac{1}{4}\,\mathrm{Im}\left\{\int_{\Gamma_D}\left[\overline{\psi(y,z)}\frac{\partial J_d(z,y)}{\partial\nu} - \frac{\partial\overline{\psi(y,z)}}{\partial\nu(y)} J_d(z,y)\right] ds(y)\right\} + R_{\hat{I}}(z), \tag{4.27}$$

where since $w(y,z) = 0$ on Γ_D,

$$\begin{aligned}R_{\hat{I}}(z) = &-\frac{1}{4}\,\mathrm{Im}\int_{\Gamma_D}\frac{\partial\overline{w(y,z)}}{\partial\nu(y)} J_d(z,y)ds(y)\\ &+\frac{1}{4}\,\mathrm{Im}\int_{\Gamma_D}\left[\overline{w_d(y,z)}\frac{\partial J_d(z,y)}{\partial\nu(y)} - \frac{\partial\overline{w_d(y,z)}}{\partial\nu(y)} J_d(z,y)\right] ds(y).\end{aligned}$$

By (4.25)-(4.26) and Corollaries 3.1-3.2 it is easy to see that

$$|R_{\hat{I}}(z)| \le C(1+kd_D)^4((kh)^{-1/2} + h/d). \tag{4.28}$$

Finally, by (4.27) and $\psi(y,z) = -\overline{F(z,y)}$ on Γ_D, we have

$$\hat{I}_d(z) = -\frac{1}{4}\,\mathrm{Im}\int_{\Gamma_D}\frac{\partial(\overline{F(z,y)} + \psi(y,z))}{\partial\nu(y)}\psi(y,z)ds(y) + R_{\hat{I}}(z) + w_{\hat{I}}(z),$$

where

$$w_{\hat{I}}(z) = 4\,\mathrm{Im}\int_{\Gamma_D}\Big[\overline{\psi(y,z)}\frac{\partial(J_d(z,y) - F(z,y))}{\partial\nu(y)} - \frac{\partial\overline{\psi(y,z)}}{\partial\nu(y)}(J_d(z,y) - F(z,y))\Big]ds(y).$$

By Lemma 4.1, Corollary 3.1 and Corollary 3.2 we have

$$|w_{\hat{I}}(z)| \leq C(1+kd_D)^4((kh)^{-1/2}+h/d).$$

This completes the proof by using (4.28). □

By (3.12) we know that for any fixed $z \in \Omega$, $\overline{F(z,\cdot)}$ satisfies the Helmholtz equation. Thus $\psi(y,z)$ can be viewed as the scattering solution of the Helmholtz equation with the incident wave $\overline{F(z,y)}$. By Lemma 3.3 we know that $\overline{F(z,y)}$ decays as $|y-z|$ becomes large. Therefore the imaging function $\hat{I}_d(z)$ becomes small when z moves away from the boundary Γ_D outside the scatterer D if $kh \gg 1$ and $d \gg h$.

To understand the behavior of the imaging function when z is close to the boundary of the scatterer, we introduce the concept of the scattering coefficient for incident plane waves.

Definition 4.1 *For any unit vector $\eta \in \mathbb{R}^2$, let $v^i = e^{\mathbf{i}kx\cdot\eta}$ be the incident wave and $v^s = v^s(x,\eta)$ be the radiation solution of the Helmholtz equation:*

$$\Delta v^s + k^2 v^s = 0 \ \text{ in } \mathbb{R}^2\backslash\bar{D}, \quad v^s = -e^{\mathbf{i}kx\cdot\eta} \ \text{ on } \Gamma_D.$$

The scattering coefficient $R(x,\eta)$ for $x \in \Gamma_D$ is defined by the relation

$$\frac{\partial(v^s+v^i)}{\partial\nu} = \mathbf{i}kR(x,\eta)e^{\mathbf{i}kx\cdot\eta} \quad \text{on } \Gamma_D.$$

It is clear that the scattering coefficient $R(x,\eta)$ is well defined by the uniqueness and existence of the solution of the Helmholtz scattering problems. One can define analogously the scattering coefficients for penetrable scatterers or non-penetrable scatterers with sound hard or impedance boundary conditions. We also remark that the scattering coefficient is closely related to the concept of reflection coefficients that are widely used in the geophysics literature in different context based on geometric optics approximations.

Now we consider the physical interpretation of the imaging function $\hat{I}_d(z)$ when $z \in \Gamma_D$. Since

$$\overline{F(z,y)} = \frac{\mathbf{i}}{2\pi}\int_0^\pi e^{\mathbf{i}k(y-z)\cdot\eta_\theta}d\theta, \quad \eta_\theta := (\cos\theta,\sin\theta)^T,$$

we obtain from Theorem 4.2 and Definition 4.1 that

$$\hat{I}_d(z) = -\frac{k}{8\pi}\mathrm{Im}\int_{\Gamma_D}\int_0^\pi \overline{F(z,y)}R(y,\eta_\theta)e^{\mathbf{i}k(y-z)\cdot\eta_\theta}d\theta ds(y) + O\left(\frac{1}{\sqrt{kh}}+\frac{h}{d}\right). \quad (4.29)$$

The main contribution in the above integral comes from $y \in \Gamma_D$ around z due to the property of the function $\overline{F(z,y)}$ studied in section 3. This indicates that the imaging function $\hat{I}_d(z)$ is proportional to the scattering coefficient surrounding z from all directions η_θ, $0 < \theta < \pi$, that is, the imaging function can be regard as "blurred scattering coefficient".

Now we consider the high frequency limit when $k \gg 1$ by the method of stationary phase. The following theorem of the stationary phase is well-known, see e.g. in [13, Theorem 7.7.5].

Lemma 4.2 *Let $g \in C_0^2(\mathbb{R})$ and the phase function $f \in C^2(\mathbb{R})$ has a stationary point at t_0 such that $f'(t_0) = 0$, $f''(t_0) \neq 0$, and $f'(t) \neq 0$ for $t \neq t_0$. Then for any $\lambda > 0$, there is a constant C such that*

$$\left| \int_{\mathbb{R}} g(t) e^{\mathbf{i}\lambda f(t)} dt - g(t_0) e^{\mathbf{i}\lambda f(t_0)} \left(\frac{\lambda f''(t_0)}{2\pi \mathbf{i}} \right)^{-1/2} \right| \leq C\lambda^{-1} \|g''\|_{C(\mathbb{R})}.$$

For simplicity we assume D is strictly convex. Let $y(s)$ be the arc length parametrization of the boundary Γ_D, $0 < s < L$. The phase function $f(s) = (y(s) - z) \cdot \eta_\theta$ satisfies $f'(s) = y'(s) \cdot \eta_\theta$, $f''(s) = y''(s) \cdot \eta_\theta$. Let $y_\pm(\eta_\theta) = y(s_\pm)$ be the points on Γ_D such that $\nu(y(s_\pm)) = \pm\eta_\theta$. Clearly we have $f'(s_\pm) = \pm y'(s_\pm) \cdot \nu(y(s_\pm))$, $f''(s_\pm) = \pm y''(s_\pm) \cdot \nu(y(s_\pm)) = \pm\kappa(y(s_\pm))|y'(s_\pm)|^2$, where κ is the curvature of Γ_D. By using the stationary phase Lemma 4.2 we have

$$\begin{aligned}
&\int_{\Gamma_D} \overline{F(z,y)} R(y,\eta_\theta) e^{\mathbf{i}k(y-z)\cdot\eta_\theta} ds(y) \\
&\approx \overline{F(z, y_+(\eta_\theta))} R(y_+(\eta_\theta), \eta_\theta) e^{\mathbf{i}k(y_+(\eta_\theta)-z)\cdot\eta_\theta} \left(\frac{k\kappa(y_+(\eta_\theta))}{2\pi\mathbf{i}} \right)^{-1/2} \\
&+ \overline{F(z, y_-(\eta_\theta))} R(y_-(\eta_\theta), \eta_\theta) e^{\mathbf{i}k(y_-(\eta_\theta)-z)\cdot\eta_\theta} \left(\frac{-k\kappa(y_-(\eta_\theta))}{2\pi\mathbf{i}} \right)^{-1/2}.
\end{aligned}$$

Thus,

$$\begin{aligned}
\hat{I}_d(z) \approx\ & -\Big(\frac{k}{32\pi}\Big)^{1/2} \mathrm{Im} \int_0^\pi \frac{\overline{F(z, y_+(\eta_\theta))} R(y_+(\eta_\theta), \eta_\theta)}{\sqrt{\kappa(y_+(\eta_\theta))}} e^{\mathbf{i}k(y_+(\eta_\theta)-z)\cdot\eta_\theta + \mathbf{i}\frac{\pi}{4}} d\theta \\
& - \Big(\frac{k}{32\pi}\Big)^{1/2} \mathrm{Im} \int_0^\pi \frac{\overline{F(z, y_-(\eta_\theta))} R(y_-(\eta_\theta), \eta_\theta)}{\sqrt{\kappa(y_-(\eta_\theta))}} e^{\mathbf{i}k(y_-(\eta_\theta)-z)\cdot\eta_\theta - \mathbf{i}\frac{\pi}{4}} d\theta.
\end{aligned}$$

This formula indicates that the imaging function $\hat{I}_d(z)$ is related to $\frac{R(z,\eta_\theta)}{\sqrt{\kappa(z)}}$, both the scattering coefficient and the curvature at z, by the property of $\overline{F(z,y)}$ studied in section 3.

In the case of Kirchhoff high frequency approximation, see e.g. [2] and the mathematical justification for strictly convex obstacles in [15], the scattering coefficient can be approximated by

$$R(x,\eta) = \begin{cases} 2\nu(x)\cdot\eta & \text{If } x \in \partial D_\eta^- := \{x \in \Gamma_D : \nu(x)\cdot\eta < 0\}, \\ 0 & \text{If } x \in \partial D_\eta^+ := \{x \in \Gamma_D : \nu(x)\cdot\eta > 0\}. \end{cases}$$

Here ∂D_η^- and ∂D_η^+ are respectively the illuminating and shadow region for the incident wave $e^{\mathbf{i}kx\cdot\eta}$. This implies, since $R(y_+(\eta_\theta), \eta_\theta) = 0$, $R(y_-(\eta_\theta), \eta) = -2$,

$$\hat{I}_d(z) \approx \Big(\frac{k}{8\pi}\Big)^{1/2} \mathrm{Im} \int_0^\pi \frac{F(z, y_-(\eta_\theta))}{\sqrt{\kappa(y_-(\eta_\theta))}} e^{\mathbf{i}k(y_-(\eta_\theta)-z)\cdot\eta_\theta - \mathbf{i}\frac{\pi}{4}} d\theta.$$

Now for z in the part of Γ_D which is back to Γ_0 , i.e. $\nu(z)\cdot\eta_\theta > 0$ for any $\theta \in]0,\pi[$, we know that z and $y_-(\eta_\theta)$ are far away and thus $\hat{I}_d(z) \approx 0$. This means one cannot image the back part of the obstacle with only the data collected on Γ_0. This is confirmed in our numerical examples in section 6.

5. Extensions

In this section we consider the reconstruction of non-penetrable obstacles with the impedance boundary condition and penetrable obstacles in the half space by our RTM algorithm 2.1. For non-penetrable obstacles with the impedance boundary condition on the obstacle, the measured data $u^s(x_r, x_s) = u(x_r, x_s) - N(x_r, x_s)$, where $u^s(x, x_s)$ is the radiation solution of the following problem:

$$\Delta u^s + k^2 u^s = 0 \qquad \text{in } \mathbb{R}^2_+ \backslash \bar{D}, \tag{5.30}$$

$$\frac{\partial u^s}{\partial \nu} + \mathbf{i}k\eta(x)u^s = -\left(\frac{\partial}{\partial \nu} + \mathbf{i}k\eta(x)\right) N(x, x_s) \qquad \text{on } \Gamma_D, \tag{5.31}$$

$$\frac{\partial u^s}{\partial x_2} = 0 \quad \text{on } \Gamma_0. \tag{5.32}$$

By modifying the argument in Theorem 4.2 we can show the following result whose proof is omitted.

Theorem 5.1 *For any $z \in \Omega$, let $\psi(y, z)$ be the radiation solution of the problem*

$$\Delta_y \psi(y, z) + k^2 \psi(y, z) = 0 \qquad \text{in } \mathbb{R}^2_+ \backslash \bar{D},$$

$$\frac{\partial \psi(y, z)}{\partial \nu(y)} + \mathbf{i}k\eta(y)\psi(y, z) = -\Big(\frac{\partial}{\partial \nu(y)} + \mathbf{i}k\eta(y)\Big)\overline{F(z, y)} \quad \text{on } \Gamma_D.$$

Then we have, for any $z \in \Omega$,

$$\hat{I}_d(z) = -\frac{1}{4}\,\mathrm{Im} \int_{\partial D} \Big(\frac{\partial \overline{F(z, y)}}{\partial \nu(y)} + \mathbf{i}k\eta(y)\overline{F(z, y)}\Big)(\psi(y, z) + \overline{F(z, y)})ds(y) + W_{\hat{I}}(z),$$

where $|W_{\hat{I}}(z)| \le C(1 + kd_D)^4((kh)^{-1/2} + h/d)$ uniformly for z in Ω.

For the penetrable obstacle, the measured data $u^s(x_r, x_s) = u(x_r, x_s) - N(x_r, x_s)$, where $u^s(x, x_s)$ is the radiation solution of the following problem:

$$\Delta u^s + k^2 n(x) u^s = -k^2(n(x) - 1)N(x, x_s) \qquad \text{in } \mathbb{R}^2_+, \tag{5.33}$$

$$\frac{\partial u^s}{\partial x_2} = 0 \qquad \text{on } \Gamma_0, \tag{5.34}$$

where $n(x) \in L^\infty(\mathbb{R}^2_+)$ is a positive function which is equal to 1 outside the scatterer D. By modifying the argument in Theorem 4.2, the following theorem can be proved.

Theorem 5.2 *For any $z \in \Omega$, let $\psi(y, z)$ be the radiation solution of the problem*

$$\Delta_y \psi(y, z) + k^2 n(y)\psi(y, z) = -k^2(n(y) - 1)\overline{F(z, y)} \quad \text{in } \mathbb{R}^2_+.$$

Then we have, for any $z \in \Omega$,

$$\hat{I}_d(z) = -\frac{1}{4}\,\mathrm{Im} \int_D k^2(1 - n(y))(\psi(y, z) + \overline{F(z, y)})\overline{F(z, y)}dy + W_{\hat{I}}(z),$$

where $|W_{\hat{I}}(z)| \le C(1 + kd_D)^4((kh)^{-1/2} + h/d)$ uniformly for z in Ω.

We remark that for the penetrable scatterers, $\psi(y, z)$ is again the scattering solution with the incoming field $\overline{F(z, y)}$. Therefore we again expect the imaging function $\hat{I}_d(z)$ will have contrast on the boundary of the scatterer and decay outside the scatterer if $kh \gg 1$ and $d \gg h$.

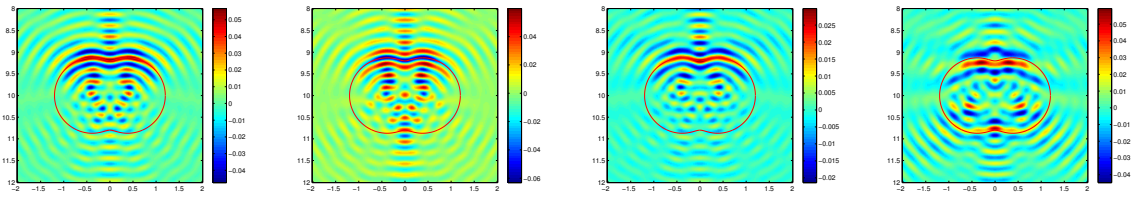

Figure 2. From left to right: imaging results of a sound soft, a sound hard, a non-penetrable obstacle with the impedance $\eta(x) = 2$, and a penetrable obstacle with the diffractive index $n(x) = 0.5$.

6. Numerical experiments

In this section we present several numerical examples to show the effectiveness of our RTM method. To synthesize the scattering data we compute the solution $u^s(x_r, x_s)$ of the scattering problem by representing the ansatz solution as the double layer potential with the Green function $N(x, y)$ as the kernel and discretizing the integral equation by standard Nyström methods [10]. The boundary integral equations on Γ_D are solved on a uniform mesh over the boundary with ten points per probe wavelength. The sources and receivers are both placed on the surface Γ_0^d with equal-distribution, where d is the aperture. In all our numerical examples we choose $h = 10$ and $d = 50$. The boundaries of the obstacles used in our numerical experiments are parameterized as follows, where $\theta \in [0, 2\pi]$,

$$\begin{aligned}
&\text{Circle:} && x_1 = \rho\cos(\theta), \quad x_2 = \rho\sin(\theta);\\
&\text{Penut:} && x_1 = \cos(\theta) + 0.2\cos(3\theta), \quad x_2 = \sin(\theta) + 0.2\sin(3\theta);\\
&\text{Kite:} && x_1 = \cos(\theta) + 0.65\cos(2\theta) - 0.65, \quad x_2 = 1.5\sin(\theta);
\end{aligned}$$

Example 6.1 We consider imaging of a sound soft, a sound hard, a non-penetrable obstacle with the impedance condition, and a penetrable obstacle. The imaging domain is $\Omega = (-2, 2) \times (8, 12)$ with the sampling grid 201×201 and $N_s = N_r = 401$. The wavenumber is $k = 4\pi$.

The imaging results are shown in Figure 2. It demonstrates clearly that our RTM algorithm can effectively image the upper boundary illuminated by the sources and receivers distributed along the boundary Γ_0 for non-penetrable obstacles. The imaging values decrease on the shadow part of the obstacles and at the points away from the boundary of the obstacle. This confirms with our theoretical results in section 4 and section 5. The last picture shows that our imaging algorithm can also locate part of the lower boundaries for penetrable obstacles.

Example 6.2 We consider the imaging of two sound soft obstacles. The first model consists of two circles along horizontal direction and the second one is a circle and a peanut along the vertical direction. The wavenumber is $k = 4\pi$ for the test of the single

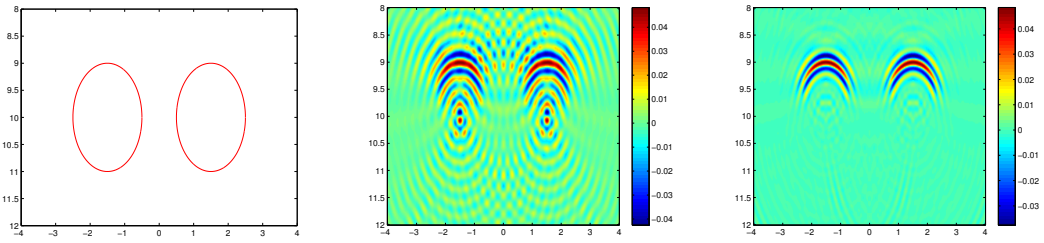

Figure 3. From left to right, true obstacle model with two circles, the imaging result with single frequency, the imaging result with multiple frequencies.

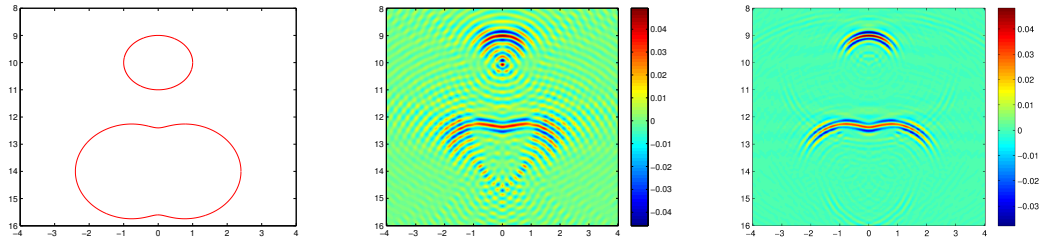

Figure 4. From left to right, true obstacle model with one circle and one peanut, the imaging result with single frequency, the imaging result with multiple frequencies.

frequency and the probed wavenumbers $k = 2\pi \times (2 + (i-1)/8), i = 1, 2, ..., 9$, for the test of multiple frequencies. Figure 3 shows the imaging result of the first model. The imaging domain is $[-4, 4] \times [8, 12]$ with mesh size 401×201 and $N_s = N_r = 301$. Figure 4 shows the imaging result of the second model. The imaging domain is $[-4, 4] \times [8, 16]$ with mesh size 201×401 and $N_s = N_r = 301$. The multi-frequency RTM imaging results in Figure 3 and Figure 4 are obtained by adding the imaging results from different frequencies and then dividing the number of the used frequencies. We observe from these two figures that imaging results can be greatly improved by stacking the multiple single frequency imaging results.

Example 6.3 In this example we consider the stability of our half space RTM imaging function with respect to the complex additive Gaussian random noise. We introduce the additive Gaussian noise as follows [5]:

$$u_{noise} = u_s + \nu_{\text{noise}},$$

where u_s is the synthesized data and ν_{noise} is the Gaussian white noise with mean zero and standard deviation μ multiplied by the maximum of the data $|u_s|$, i.e. $\nu_{\text{noise}} = \frac{\mu \max |u_s|}{\sqrt{2}}(\varepsilon_1 + \mathbf{i}\varepsilon_2)$, and $\varepsilon_j \sim \mathcal{N}(0, 1)$ for the real $(j = 1)$ and imaginary part $(j = 2)$.

Figure 5 shows the imaging results using single frequency data added with additive Gaussian noise. The imaging quality can be improved by using multi-frequency data as illustrated in Figure 6, in which we show the imaging results added with the noise

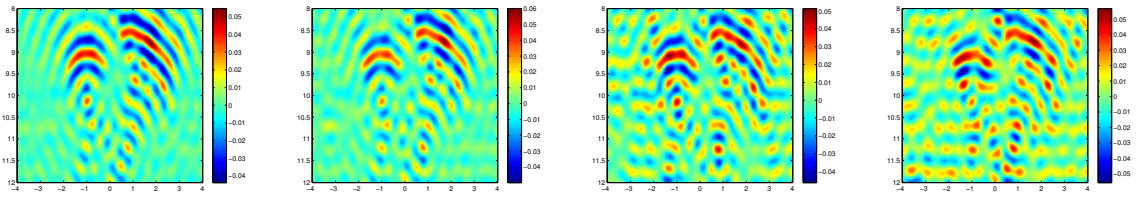

Figure 5. The imaging results using single frequency data added with additive Gaussian noise and $\mu = 10\%, 20\%, 40\%, 60\%$ from left to right, respectively. The probe wavenumbers are $k = 2\pi$ and $N_s = N_r = 301$.

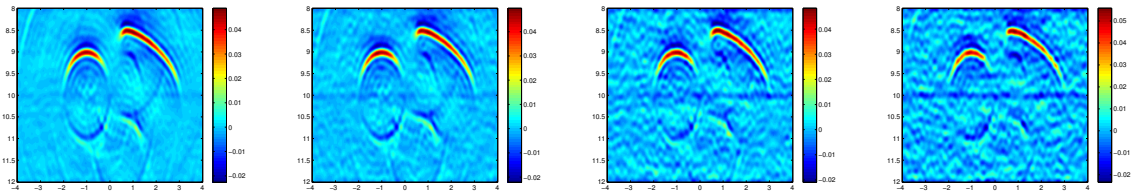

Figure 6. The imaging results using multi-frequency data added with additive Gaussian noise and $\mu = 10\%, 20\%, 40\%, 60\%$ from left to right, respectively. The probe wavenumbers are $k = \pi \times (1 + (i-1)/4), i = 1, 2, ..., 9$, and $N_s = N_r = 301$.

Table 1. The signal level and noise level in the case of single frequency data (left) and multi-frequency data (right).

μ	σ	$\|u_s\|_{\ell^2}$	$\|\nu_{\text{noise}}\|_{\ell^2}$
0.1	0.0639	0.0136	0.0522
0.2	0.1279	0.0136	0.1045
0.4	0.2558	0.0136	0.2086
0.6	0.3836	0.0136	0.3127

μ	σ	$\|u_s\|_{\ell^2}$	$\|\nu_{\text{noise}}\|_{\ell^2}$
0.1	0.0593	0.0126	0.0484
0.2	0.1185	0.0126	0.0967
0.4	0.2370	0.0126	0.1936
0.6	0.3555	0.0126	0.2902

level $\mu = 10\%, 20\%, 40\%, 60\%$ Gaussian noise by summing the imaging functions for nine probed wavenumbers $k = \pi \times (1 + (i-1)/4), i = 1, 2, ..., 9$.

The left table in Table 1 shows the noise level in this case, where $\sigma = \mu \max_{x_r, x_s} |u^s(x_s, x_r)|$, $\|u_s\|^2_{\ell^2} = \frac{1}{N_s N_r} \sum_{s,r=1}^{N_s,N_r} |u^s(x_s, x_r)|^2$, $\|\nu_{\text{noise}}\|^2_{\ell^2} = \frac{1}{N_s N_r} \sum_{s,r=1}^{N_s,N_r} |\nu_{\text{noise}}(x_s, x_r)|^2$. The right table in Table 1 shows the noise level in the case of multi-frequency data, where σ, $\|u_s\|_{\ell^2}$, and $\|\nu_{\text{noise}}\|_{\ell^2}$ are the arithmetic mean of the corresponding values for different frequencies, respectively.

Appendix A. The proof of Theorem 4.1.

We first recall the following Van der Corput lemma, see e.g. in [12, Corollary 2.6.8], which is useful to estimate the oscillatory integral around the critical point.

Lemma A.1 *There is a constant $C > 0$ such that for any $-\infty < a < b < \infty$, for every real-valued C^2 function u that satisfies $u''(t) \geq 1$ for $t \in]a, b[$, for any function ϕ defined on $]a, b[$ with an integrable derivative, and for any $\lambda > 0$,*

$$\left| \int_a^b e^{\mathbf{i}\lambda u(t)} \phi(t) dt \right| \leq C\lambda^{-1/2} \left(|\phi(b)| + \int_a^b |\phi'(t)| dt \right),$$

where the constant C is independent of the constants a, b, λ and the functions u, ϕ.

Lemma A.2 *For any $x, y \in \Omega$, there exists a constant $C > 0$ independent of k, h such that for $m = 1, 2, 3$, $n = 1, 2$,*

$$\Big| \int_{\Gamma_0} \Big(\frac{y_2^m}{|\xi - y|^{m+1}} + \frac{(\xi_1 - y_1)^2 y_2^n}{|\xi - y|^{n+3}} \Big) e^{\mathbf{i}k(|\xi - x| + |\xi - y|)} ds(\xi) \Big| \leq C(kh)^{-1/2}.$$

Proof. For simplicity, we only prove the estimate when $m = 1$. The other estimates can be obtained similarly. By the change of variable $t = (\xi_1 - y_1)/y_2$ we know that

$$\int_{\Gamma_0} \frac{y_2}{|\xi - y|^2} e^{\mathbf{i}k(|\xi - x| + |\xi - y|)} ds(\xi) = \int_{-\infty}^{\infty} \frac{1}{1 + t^2} e^{\mathbf{i}k y_2 f(t)} dt, \tag{A.1}$$

where $f(t) = \sqrt{1 + t^2} + \sqrt{(t + a)^2 + b^2}$, $a = (y_1 - x_1)/y_2$, $b = x_2/y_2$. By the second inequality in the assumption (2.4), $|a| \leq c_1 b$ for some $c_1 > 0$. Simple calculation shows that

$$f'(t) = \frac{t}{\sqrt{1 + t^2}} + \frac{t + a}{\sqrt{(t + a)^2 + b^2}}, \quad f''(t) = \frac{1}{(1 + t^2)^{3/2}} + \frac{b^2}{((t + a)^2 + b^2)^{3/2}}.$$

It is easy to check that $f'(t)$ is strictly increasing and $f'(t_0) = 0$, $t_0 = -a/(1 + b)$. In the interval where $|t + a| < c_1 b$ we know that $f''(t) \geq b^{-1}(1 + c_1^2)^{-3/2} \geq C$ and thus by Lemma A.1

$$\left| \int_{-a - c_1 b}^{-a + c_1 b} \frac{1}{1 + t^2} e^{\mathbf{i}k y_2 f(t)} dt \right| \leq C(kh)^{-1/2}. \tag{A.2}$$

In the intervals where $|t + a| \geq c_1 b$, since $f'(t)$ is increasing,

$$|f'(t)| \geq \min(|f'(-a + c_1 b)|, |f'(-a - c_1 b)|) \geq \frac{c_1}{\sqrt{1 + c_1^2}}.$$

Thus by integration by parts one can obtain the following estimate by the standard argument

$$\left| \int_{(-\infty, -a - c_1 b) \cup (-a + c_1 b, \infty)} \frac{1}{1 + t^2} e^{\mathbf{i}k y_2 f(t)} dt \right| \leq C(kh)^{-1}. \tag{A.3}$$

This completes the proof by substituting (A.2)-(A.3) into (A.1). □

Lemma A.3 *For any $x, y \in D$, let*

$$v(x, y) = \int_{\Gamma_0} \Phi(x, \xi) \frac{\partial \Phi(\xi, y)}{\partial \xi_2} ds(\xi).$$

Then there exists a constant $C > 0$ independent of k, h such that

$$|v(x, y)| + k^{-1} |\nabla_x v(x, y)| + k^{-1} |\nabla_y v(x, y)| + k^{-2} |\nabla_x \nabla_y v(x, y)| \leq C(1 + k d_D)(kh)^{-1/2},$$

uniformly for $x, y \in D$.

Proof. By using the asymptotic formula for the Hankel functions

$$H_j^{(1)}(t) = \left(\frac{2}{\pi t}\right)^{1/2} e^{\mathbf{i}(t-\frac{\pi}{4}-\frac{j}{2}\pi)} + R_j(t), \quad |R_j(t)| \le Ct^{-3/2}, \quad \forall t > 0, \quad j = 0, 1, \tag{A.4}$$

we obtain by using (3.18)

$$v(x,y) = -\frac{1}{8\pi}\int_{\Gamma_0} \frac{y_2}{|\xi-y|^{3/2}|\xi-x|^{1/2}} e^{\mathbf{i}k(|\xi-y|+|\xi-x|)} ds(\xi) + \gamma(x,y), \tag{A.5}$$

where

$$\gamma(x,y) \le C\int_{\Gamma_0} \frac{y_2}{k|\xi-y|^3} ds(\xi) \le C(kh)^{-1}.$$

Notice that $||\xi-y|^{-1/2} - |\xi-x|^{-1/2}| \le C|x-y|/|\xi-y|^3$ for any $x, y \in D$, $\xi \in \Gamma_0$, we have

$$\begin{aligned} &\left|\int_{\Gamma_0} \frac{y_2}{|\xi-y|^{3/2}|\xi-x|^{1/2}} e^{\mathbf{i}k(|\xi-y|+|\xi-x|)} ds(\xi)\right| \\ &\le \left|\int_{\Gamma_0} \frac{y_2}{|\xi-y|^2} e^{\mathbf{i}k(|\xi-y|+|\xi-x|)} ds(\xi)\right| + C\int_{\Gamma_0} \frac{y_2|x-y|}{|\xi-y|^3} ds(\xi). \end{aligned}$$

By the change of variable $t = (\xi_1 - y_1)/y_2$ we obtain

$$\int_{\Gamma_0} \frac{y_2|x-y|}{|\xi-y|^3} ds(\xi) = \int_{-\infty}^{\infty} \frac{|x-y|}{y_2(1+t^2)^{3/2}} dt \le C\frac{|x-y|}{y_2} \le C(kd_D)(kh)^{-1}.$$

This completes the proof of the estimate for $|v(x,y)|$ by using Lemma A.2. The other estimates can be proved by a similar argument using Lemma A.2. We omit the details. □

Now we are ready to prove Theorem 4.1.

Proof of Theorem 4.1. Let w be the radiation solution of the problem:

$$\Delta w + k^2 w = 0 \ \text{ in } \mathbb{R}^2_+, \qquad \frac{\partial w}{\partial x_2} = -\frac{\partial u_2}{\partial x_2} \ \text{ on } \Gamma_0.$$

Then $u_1 - u_2 - w$ satisfies (4.19) with the boundary condition $u_1 - u_2 - w = -w$ on Γ_D. Thus by Lemma 4.1 and (3.14)-(3.15) we obtain

$$\begin{aligned} \|\partial(u_1-u_2)/\partial\nu\|_{H^{-1/2}(\Gamma_D)} &\le C(\|w\|_{H^{1/2}(\Gamma_D)} + \|\partial w/\partial\nu\|_{H^{-1/2}(\Gamma_D)}) \\ &\le C\max_{x\in D}(|w(x)| + d_D|\nabla w(x)|). \end{aligned}$$

By the integral representation formula we have for any $\xi \in \Gamma_0$

$$u_2(\xi) = \int_{\Gamma_D} \left[u_2(y)\frac{\partial\Phi(y,\xi)}{\partial\nu(y)} - \frac{\partial u_2(y)}{\partial\nu(y)}\Phi(y,\xi)\right] ds(y),$$

which yields by using the integral representation again that for $x \in D$,

$$\begin{aligned} w(x) &= \int_{\Gamma_0} N(x,\xi)\frac{\partial u_2(\xi)}{\partial\xi_2} ds(\xi) \\ &= 2\int_{\Gamma_D} \left[u_2(y)\frac{\partial v(x,y)}{\partial\nu(y)} - \frac{\partial u_2(y)}{\partial\nu(y)} v(x,y)\right] ds(y), \end{aligned}$$

where we have used the fact that $N(\xi, x) = 2\Phi(\xi, x)$ for $\xi \in \Gamma_0$. Therefore, since $\|\partial u_2/\partial\nu\|_{H^{-1/2}(\Gamma_D)} \leq C\|g\|_{H^{1/2}(\Gamma_D)}$, we obtain by using (3.14) again

$$|w(x)| \leq C\|g\|_{H^{1/2}(\Gamma_D)} \max_{y\in D}(|v(x,y)| + d_D|\nabla_y v(x,y)|).$$

Similarly, we have

$$|\nabla w(x)| \leq C\|g\|_{H^{1/2}(\Gamma_D)} \max_{y\in D}(|\nabla_x v(x,y)| + d_D|\nabla_x\nabla_y v(x,y)|).$$

This completes the proof by using Lemma A.3. □

Acknowledgments

This work is supported by National Basic Research Project under the grant 2011CB309700 and China NSF under the grants 11021101 and 11321061. The authors would like to thank Dr. Yu Zhang from ConocoPhillips for inspiring discussions and the referees for their helpful comments.

References

[1] H. Ammari, J. Garnier, W. Jing, H. Kang, M. Lim, K. Solna, and H. Wang 2013 *Mathematical and Statistical Methods for Multistatic Imaging* (Springer)

[2] Bleistein N, Cohen J and Stockwell J 2001 *Mathematics of Multidimensional Seismic Imaging, Migration, and Inversion* (New York: Springer)

[3] Berkhout A 1984 *Seismic Migration: Imaging of Acoustic Energy by Wave Field Extrapolation* (New York: Elsevier)

[4] Chandler-Wilde S N, Graham I G, Langdon S and Lindner M 2009 Condition number estimates for combined potential boundary integral operators in acoustic scattering *J. Integral Equa. Appli.* **21** 229-279.

[5] Chen J, Chen Z and Huang G 2013 Reverse time migration for extended obstacles: acoustic waves *Inverse Problems* **29** 085005 (17pp)

[6] Chen J, Chen Z and Huang G 2013 Reverse time migration for extended obstacles: electromagnetic waves *Inverse Problems* **29** 085006 (17pp)

[7] Chen Z and Huang G 2014 Reverse time migration for reconstructing extended obstacles in planar acoustic waveguides arXiv:1406.4768

[8] Chew W C 1990 *Waves and Fields in Inhomogeneous Media* (New York: IEEE Press)

[9] Claerbout J F 1985 *Imaging the Earth's Interior* (Oxford: Blackwell Scientific Publication)

[10] Colton D and Kress R 1998 *Inverse Acoustic and Electromagnetic Scattering Problems* (Heidelberg: Springer)

[11] Dominguez V, Graham I G and Smyshlyaev V P 2007 A hybrid numerical-asymptotic boundary integral method for high-frequency acoustic scattering *Numerische Mathematik* **106** 471-510

[12] Grafakos L 2004 *Classical and Modern Fourier Analysis* (London: Pearson)

[13] Hörmander L 1983 *The Analysis of Linear Partial Differential Operators, I* (Berlin: Springer)

[14] Leis R 1986 *Initial Boundary Value Problems in Mathematical Physics* (Stuttgart: B.G. Teubner)

[15] Melrose R B and Taylor M E 1985 Near peak scattering and the corrected Kirchhoff approximation for a convex obstacle *Advances in Mathematics* **55** 242-315

[16] Stein E M and Timothy S M 1993 *Harmonic Analysis: Real-Variable Methods, Orthogonality, and Oscillatory integrals* (Princeton: Princeton University Press)

[17] Watson G N 1922 *A Treatise on the Theory of Bessel Functions* (Cambridge: Cambridge University Press)

[18] Zhang Y and Sun J 2009 Practicle issues in reverse time migration: true amplitude gathers, noise removal and harmonic source encoding *First Break* **26** 29-35

[19] Zhang Y, Xu S, Bleistein N and Zhang G 2007 True-amplitude, angle-domain, common-image gathers from one-way wave-equation migration *Geophysics* **72** S49-S58